Data Analytics and Artificial Intelligence

Vol: 3(2), 2023

REST Publisher; ISBN: 978-81-948459-4-2

Website: http://restpublisher.com/book-series/daai/

DOI: https://doi.org/10.46632/daai/3/2/39

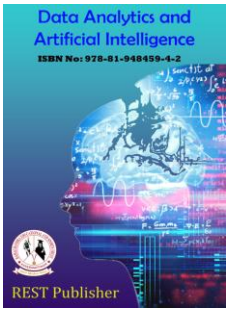

Investigation of Stress Distribution in a Railway Embankment Reinforced By Geogrid Based Weak Soil Formation Using Hybrid Rnn-Eho

***M.A.Balasubramani, R.Venkatakrishnaiah, K.V.B.Raju**

Bharath Institute of Higher Education and Research, Tamil Nadu, India.

*Corresponding Author Email: mabalacivil@gmail.com

Abstract: *As the primary method of track support, traditional sloping embankments are typically used by railroad lines. Geosynthetically Reinforced Soil (GRS) systems, as an alternative to traditional embankments, have gained appeal, notably for high-speed lines in India. This system's reduced base area compared to traditional embankments means that less ground stabilization, improvement, and land taking is necessary. The research's findings provide intriguing strategies that may be implemented into the way tracks are designed now to accommodate faster freight trains pulling greater loads. This research explains how to anticipate the bearing capacity of weak sand supported by a method of compacted granular fill over natural clay soil using a hybrid Recurrent Neural Network (RNN) and Elephant Herding Optimization (EHO) with Georgic reinforced soil foundation. The exact prediction target for the proposed model was developed by using displacement amplitude as an output index. A number of elements influencing the foundation bed's properties, Georgic reinforcement, and dynamic excitation have been taken into account as input variables. The RNN-anticipated EHO's accuracy was compared to that of three other popular approaches, including ANN, HHO, CFA, and MOA. Strict statistical criteria and a multi-criteria approach were principally used to assess the predictive power of the developed models. The model is also examined using fresh, independent data that wasn't part of the initial dataset. The hybrid RNN-EHO model performed better in predicting the displacement amplitude of footing lying on Geogrid-reinforced beds than the other benchmark models. Last but not least, the sensitivity analysis was used to highlight how input parameters might affect the estimate of displacement amplitude.*

Keywords: *Recurrent Neural Network (RNN), Elephant Herding Optimization (EHO), Geogrid, Settlement, soil reinforcement, Weak Sand, Mayfly Optimization Algorithm, Jellyfish search algorithm, Cuttlefish algorithm and Artificial neural network*

1. INTRODUCTION

The primary component affecting high-speed train track and ground responses is the interplay of train loads and Rayleigh surface waves on the railway embankment and track bed [1-3]. One of the most crucial elements in explaining, forecasting, or predicting a track reaction and considering the proper remedial action is the bed's Rayleigh wave velocity. Studies have demonstrated the requirement for safety on soft ground railroads due to the high-speed trains' extensive range of vibration, particularly while operating at critical speed. The inherent vibrating characteristics of the rail systems define this speed. The important speed is the train speed that induces a pseudo-resonance event in the bed and is roughly equal to or larger than the Rayleigh wave speed of the bed [4, 5]. The critical speed also leads to significant track deviations, severe embankment vibration, and cone-shaped ground wave motion. The processes for bed soil augmentation are influenced by a number of variables, including train speed, soil type, embankment height, and the thickness of soft and loose sediments. Numerous methods, including geosynthetics (geogrid), vibro-replacement with stone columns, dry deep soil mixing (cement columns), concrete piles with or without integrated caps, removal replacement methods with suitable materials, and the installation of mechanical reinforcements like plate anchors and helical piles, can be used to improve the soils beneath railway embankments [6, 7].

Although georgic reinforcement has been used for many years in other geotechnical applications, there hasn't been much study on its usage in railway engineering. This could be due to the conservative nature of the sector and the lack of a design technique specialized for railway embankments [8]. Despite the fact that the reinforcement has shown to improve performance under static and cyclic loads, there is a paucity of study on where the georgic should be placed and how well it performs in a difficult environment like railway ballast. Additional knowledge of how ballast and georgic behave in a railway application may aid in the advancement of useful design techniques. In terms of cost and the environment, such an application may have an effect on future train design and track restoration [9]. To sustain the repeated stress caused by train passes, ballast acts as a foundation to absorb energy, drain easily, and withstand pressures

acting both vertically and laterally (Selig and Waters). However, significant technological issues [10] make it difficult to carry out these important duties. Train loading forces may cause ballast to be rearranged and degraded during several loading cycles, diminishing grain interlocking and allowing lateral particle migration. As ballast particles migrate laterally, track stability may suffer as a result of a reduction in frictional strength. Loss of track geometry results from vertical and lateral deformations brought on by spreading or foundation issues. Maintaining the ballasted foundation's shape is essential since track maintenance due to geotechnical issues is more costly than other track expenditures..

Numerous studies have examined the production of building materials like concrete and geopolymer bricks from waste materials, as well as how to increase the bearing capacity of shallow foundations. If we compare the reinforced case with the unreinforced one at the same load, Ziegler *et al*. [11] have shown an improvement in bearing capacity and a notable reduction in in displacements. It was shown that these results may be attributed to the georgic reinforcement's restricting action and interlocking mechanism, which bend the more or less straightdeviatoric stress route in the unreinforced case into an isotropic stress path in the reinforced case. Samples of ballasted railroad track that had been exposed to mixed vertical-horizontal cyclic stresses experienced settlement at high relative train speeds, according to Yu *et al*. [12]. The installation of georgic at the ballast-sub ballast contact, the subballast-subgrade interface, and the effect of sub grade stiffness on geogrid performance at the subballast-subgrade interface were all studied for their performance advantages. By using laboratory testing and finite element modelling, Esmaeili*et al*. [13] has shown how geogrid affects the stability and settlement of high railway embankments. This was accomplished by stacking evenly five sets of 50 cm-high embankments that were created at a scale of 1:20 on the crest of a loading chamber that was 240 x 235 x 220 cm in size. The original set of embankments weren't reinforced with any geogrid layers. A ground remediation method was put out by Zhang *et al*. [14] to lessen persistent train-induced deformation. Group piles' bearing strata received continuous injections of permeation grouting. The impact of the suggested technique's mitigation was then investigated by numerical simulations based on advanced constitutive models and soil-water coupled finite element-finite difference (FE)-(FD) compound arithmetic. According to a study by Punetha*et al*. [15] upon whether ballasted train track performance may be improved by using recycled concrete aggregates and geosynthetics. Employing two-dimensional finite element analysis, the value of using geogrids, geocells, and recycled concrete aggregates in the ballasted railway tracks is examined. The efficacy is evaluated using the track settlement. The results show that the use of geosynthetics and recycled aggregates significantly decreases track settlement and may enable higher train speeds at the same allowable settlement level.Understanding the performance mechanism of geogrid material layers used to reinforce high railway embankments is the major goal of this investigation. As influencing elements for the serviceability of railway embankments, the study's major attention is on reducing crest settling and preventing sliding in the embankment body. The results of all reinforced numerical models and preliminary numerical modelling were used to determine the proper level for installing the geogrid layers. In order to do this, the first series of embankments were built without any further geogrid reinforcement, and the second through fifth series were each reinforced with one to four layers of geogrid.

2. PROPOSED METHODOLOGY

2.1. Material properties of model clay barrier

Sand and kaolin were combined in a 4:1 dry weight ratio as the soil in the current investigation in order to mimic the clay barrier and attain the required hydraulic conductivity of 1 109 m/s. The model clay barrier material was determined to have a maximum dry unit weight of 15.9 kN/m^3, a liquid limit of 38 percent, a plastic limit of 16 percent, a coefficient of permeability of 0.4 109 m/s, and an ideal moisture content of 22 percent (standard Proctor compaction test). According to the Unified Soil Classification System (UCSC), which categorises it as a CL type, the chosen combination was found to have qualities that are equivalent to those of the majority of locally accessible naturally formed clays in the majority of India. It also illustrates clay barriers used in landfills' fine-grained soil bandwidth features [16]. It was discovered that the clay barrier, which is damp compacted at OMC+5%, has a comparable dry unit weight and shear strength of between 30 and 40 kN/m^2.

2.2. Geogrid

Bi-directional geogrids are used throughout all series of experiments. Table 1 displays the geogrid's characteristics utilised in this investigation.

TABLE 1: Geogrid index characteristics

Parameter	**Value**
Thickness (mm)	1.8
Mass per unit area (Kg/m2)	0.532
Ultimate tensile strength (kN/m)	7.6
Aperture size (mm)	23

2.3. Measuring subgrade stiffness

The stiffness and strength characteristics of the subgrade and formation were evaluated at various testing phases (the formation layer was replaced prior to each test). Unconfined compression tests were used to determine strength, and a circular plate load test was used to determine stiffness under the Losenhausen piston.These values were contrasted with

findings from studies utilising light falling deflectometers, dynamic penetration tests, and pocket penetrometers [17]. The stiffness data from the plate load test was believed to be the most reliable, and the Young's modulus was computed using:

$$S_{Plt} = \frac{2P(1-PR^2)}{\pi r \mu} \tag{1}$$

Where the plate's radius stands r, P the plate applied load, PR and μ are the Poisson's ratio and plate's deflection. The term $S_{Plt}(t)$ is used to define the tangent Young's modulus obtained from the first half of the second load cycle curve in order to avoid early setup issues (i.e. plate-surface contact errors).

There is a study of track settlement computations available; however, the presented method uses the pathlimitation (t) provided by:

$$t = \frac{S_{Pli}}{P} = \frac{Stiff}{\text{Pr}ess} \tag{2}$$

The relevant unreinforced ballast control tests in this research are designated as CT1, CT2, and CT3, along with details regarding the testing. The fact that the projected resilient modulus values for each test at the breakpoint stress often followed the same pattern as the actual plate load $S_{Plt}(t)$modulus values demonstrated the consistency of the tests.

2.4. Multi objective Function

The bad sand's stability is improved in this step using the optimization parameter of the hybrid RNN-EHO method, which is also employed to improve the appearance of the proposed Geogrid. The main goal of the suggested hybrid RNN-EHO approach in this case is to reduce the form characteristic, which is scientifically unique in equation (3),

$$OF = \Omega = Min_E(\Psi_P, \Psi_{bc}, \Psi_s) \tag{3}$$

Where, Ψ_s are the pressure and bearing capacity error minimizations and the pressure and Ψ_P, Ψ_{bc} arebearing capacity error minimizations of the weak soil formation.

2.5. Improving settlement-based Geogrid using hybrid RNN-EHO technique

Use RNN to choose the most appropriate subset of dataset attributes in this case to discriminate between susceptible and regular data. RNN mimics the creation of goal functions and feature selection. According to the same theory, an RNN enhances the answer by progressively choosing the best options while removing the less desirable ones [18]. Figure 1 shows the RNN model's architectural layout. The input layer is made up of vectors that $x, y(t), z(t)$ and $w(t-1)$ respectively, correspond to the present user, item, responseaction, and hidden layer state.The user m is referenced in the model via $l \times 1$a vector, where m^{th} element is 1 and the remaining elements are 0. An $n \times 1$ or 1×1vector refers to each item (or kind of feedback action) in the same manner. H and m stand for the user's and the item's respective hidden layers. The hidden layer's output w at the current periodstage t is referenced by the vector $w(t)$. O is the layer of output.

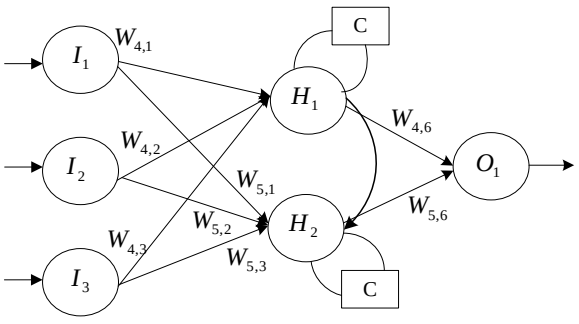

FIGURE 1: The architecture of the RNN model

Through the weight matrix A, the user vector x from the input layer is linked to the hidden layer H. This portion is non-recurring, and equation is used to compute the hidden layer's output (4),

$$H = f(Ax) \tag{4}$$

The dimension of the concealed layer H is represented by the vector $D \times 1$in this area. A is a $D \times m$ matrix with a user's choice referred to in each column. The equation provides the sigma function f as the equation (5).

$$f(x) = \frac{1}{1+e^{-x}} \tag{5}$$

The weight matrices M, N and L, respectively, link the input layer's vectors and to the hidden layer's vectors $x, y(t), z(t)$ and $w(t-1)$. The hidden layer records $s(t-1)$ prior user behaviour while this section of the model is repeated. To determine the hidden layer's output at the time stamp, $t, w(t)$ apply equation (6).

$$w(t) = f\left(Mx(t) + Ny(t) + Lw(t-1)\right) \tag{6}$$

Where, $D\times 1$a vector is $w(t)$. M, N and L are $D\times n$, $D\times 1$ and $D\times D$ are the corresponding matrices M. The feature of an item is referenced in each column of the matrix N. Additionally, each column in the matrix denotes a certain kind of feedback activity. A vector $n\times 1$ is produced by the system at the periodimprint and t, $O(t)$ is computed using equation (7),

$$O(t) = g(Ys(t) + Zh) \tag{7}$$

The weight matrices for the hidden layer and the output layer are Y and Z. The equation provides the softmax function as g.

$$g(x) = \frac{e^{x}}{\sum_{i=1}^{K} e^{x_i}} \tag{8}$$

The assessment of the likelihood that the user m would approach the item j at the following timestamp provided by the historical feedback that is calculated using equation (9) $O(t+1)$, $O_j(t+1)$ is the output element j^{th} after the network has been trained.

$$O_j(t+1) = P(v_j(t+1) = 1/x, y(t), z(t), w(t-1)) \tag{9}$$

When a proposal is executed, the output at the model's final time stamp is determined for each user. Simply choose the P output's largest items, and it is advisable to use their indexes. The Geogrid controller is then given the RNN as input based on the weak soil development in the railway track.

2.5. The procedure of the EHO inrealizing the learning of RNN

The learning function of the RNN algorithm is implemented by the EHO algorithm. The programme was inspired by the herding behavior of elephants. Due to the gregarious character of the elephant, there are several factions of female elephants in the group, each of which is carrying a calf [19]. Each group's movement is influenced by its matriarch or leader elephant. As seen in figure 2, the Female Elephant (FE) once lived with family gatherings while the Male Elephant (ME) grew up and lives alone while maintaining contact with his family group.

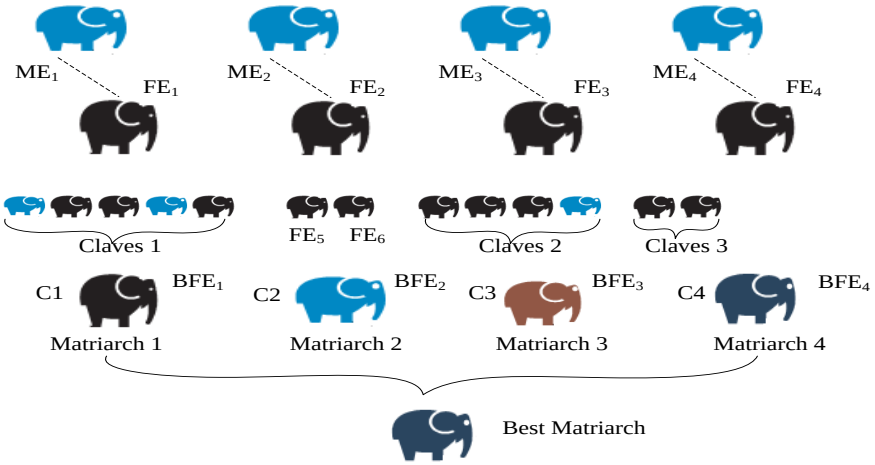

FIGURE 2: EHO Elephants' Behaviours

The following assumptions about herding are taken into consideration in EHO:

- The total elephant population is divided into clans, with each clan containing a specified number of elephants.
- A established population of ME permits their clan and life to be left alone.
- A matriarch oversees the operations of each tribe.

One can infer that there is the same number of elephants in each clan. The matriarchal group in the elephant herd is organised in the greatest way possible, whereas the male elephant herd is positioned in the worst way possible. The EHO framework or initiatives were shown as follows [20].

Step 1: Initialization Process

These procedures set the hidden layers, neurones, basis weights (which range from - 10 to +10), and reference values for the RNN using real learning function values. The EHO parameters are scaling factors and the optimisation model starts with random values.

Step 2: Process for Evaluating Fitness

The weak soil formation and EHO settling are taken into consideration by this Geogrid model. Below is the equation that is produced when this value is derived utilising the best hidden layers and RNN structure neurones.

$$FF = \Omega \quad (10)$$

Utilizing the hybrid algorithm, the fitness is attained.

Step 3: Current elephant location

The best and worst options for each elephant in each family in this third stage, with the exception of the matriarch and a male elephant, are included in the status of each elephant P and each clan C_i has elephants.The elephant's $i = 1,2,....P$ rank and j^{th} clan $j = 1,2,....C$ are symbolised by $L_{i,j}$. The elephant's current location i^{th} is stated as

$$L_{new,c_{i,j}} = L_{ci,j} + \alpha(L_{best,ci,j} - L_{ci,j}) \times r \quad (11)$$

Here $L_{newci,j} \rightarrow$ updated position, $L_{ci,j} \rightarrow$ old position, $L_{bestci,j} \rightarrow$ Position of best in the clan. α and $r \in 0 to 1$.

By following the methods above, the optimum position that reflects the matriarch cannot be modified.

Step 4: Movement update for each clan's fittest elephant

The position update for the clan member that fits in best is provided by

$$L_{new,ci,j} = \beta \times L_{center,c_j} \text{ and } L_{center,c_j} = \sum_{i=1}^{n} L_{ci,j} / n_l \quad (12)$$

Here $n_l \rightarrow$the overallquantity of elephants in individually clan and $\beta \in [0\ 1]$

Step 5: Separating the worst of the clan's elephants

Male elephants or the worst elephants would be taken away from their family groupings. the lowest ranking changed to

$$L_{worst,ci,j} = L_{\min} + (L_{\max} - L_{\min} + 1) \times r \quad (13)$$

Where $L_{worst,ci,j} \rightarrow$ the clan's worst male elephants , $L_{\max}$ *and* $L_{\min} \rightarrow$are, as well as the elephants' permitted maximum and lowest range.

Step 6: Ending procedure

It completes one iteration since the weakest elephant in the clan has been separated. The process is continued until the RNN's leaning function for settling weak soil formation is achieved, at which time it is deemed complete. If the criteria is not satisfied, then steps 2 through 6 are repeated until the convergence conditions are satisfied. Figure 3 depicts the process flow diagram for the hybrid RNN-EHO approach.

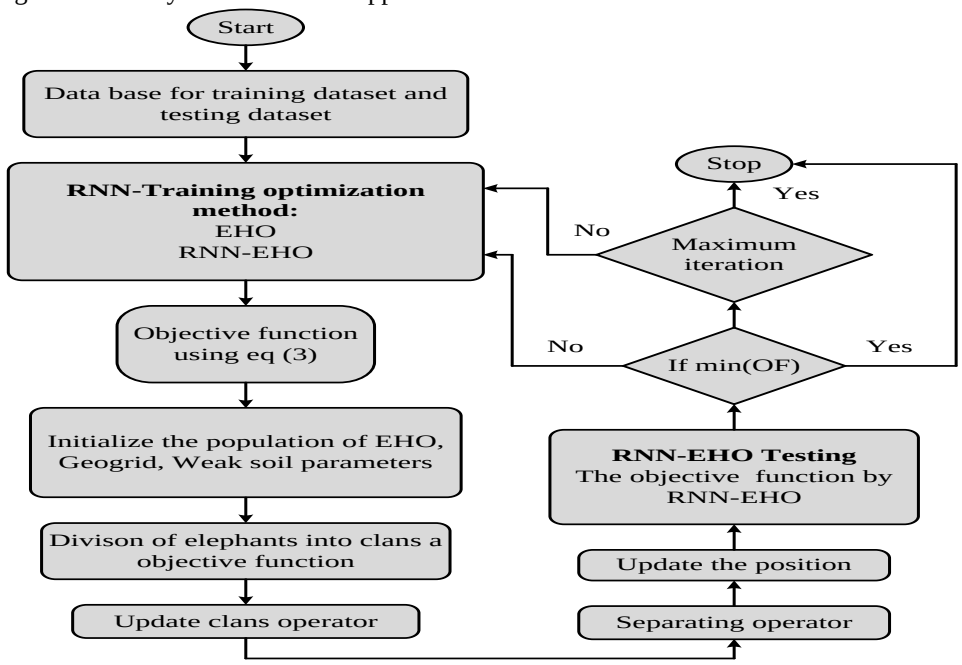

FIGURE 3: Flowchart of proposed hybrid RNN-EHO method

3. RESULTS AND DISCUSSION

Two reinforced and unreinforced examples with the test results are provided. It will be explained how bearing pressure compares to normalised settlement, how much of the load is supported by piles, and how axial stress is

distributed throughout the length of the pile. The ideal cushion thickness and pile spacing were found in the unreinforced case, while in the reinforced case, the ideal placement of the first layer of the geogrid and the ideal length of geogrids were discovered. The Geogrid sand foundations are powered by Matlab 7.10.0 (R2021a) and an Intel (R) Core (TM) i5 CPU with 4GB RAM. In order to confirm its performance, the new system was put to the test and its processing parameters were compared to a number of techniques, including the Artificial Neural Network (ANN), Harris Hawks Optimization (HHO), Cuttlefish algorithm (CFA), and Mayfly Optimization Algorithm (MOA) models.

3.1. Uncertainty analysis

Wilmot's Index of Agreement (WI), Mean Absolute Percentage Error (MAPE), Mean Absolute Percentage Error (RMSE), Mean Absolute Percentage Error (MAPE), Mean Absolute Percentage Error (RMSE), coefficient of correlation (R^2), and mean absolute error (MAE) were all calculated to evaluate the performance of the final selected architecture for the proposed ANN-MGSA (i.e., testing information that the network hasn't encountered throughout the training process). Equations (14) to (18) are used to compute the values of MAE (mean absolute error), RMSE (root-mean-square error), and R for the training and testing portions.

Five indicators were used to assess how well the suggested machine learning models performed:

RMSE: The standard errors between predicted values and actual values can be represented using RMSE. The algorithm is defined as being given in Eq and is said to be more exact the smaller the RMSE represents (14).

$$RMSE = \sqrt{\frac{1}{n}\sum_{i=1}^{n}\left(O_S^i - P_S^i\right)^2} \tag{14}$$

Correlation Coefficient (R): R measures how strongly the measured values and the variation in forecasted values are related. The R value varies from - 1 to 1, where - 1 denotes a completely inverse correlation and - 1 denotes a completely inverse correlation. The definition of R is given in Eq. (15)

$$R\left(P^i, O^i\right) = \frac{\operatorname{cov}\left(P^i, O^i\right)}{\sqrt{\operatorname{var}\left[P^i\right] * \operatorname{var}\left[O^i\right]}} \tag{15}$$

Mean Absolute Percentage Error (MAPE): A dimensionless measure called MAPE may be used to rate a model's ability to anticipate outcomes. The greater the model's derived predictive performance, the closer MAPE is to 0. Equation represents the MAPE definition (16).

$$MAPE = \frac{100\%}{n}\sum_{i=1}^{n}\frac{\left|P_S^i - O_S^i\right|}{P_S^i} \tag{16}$$

Coefficient of Determination (R^2): R^2 measures how closely the anticipated value resembles the actual value. R2 is between 0 and 1. The perfect match between the anticipated value and the actual value is shown by an R2 of 1. Equation(17) displays R^2's definition.

$$R^2 = 1 - \frac{\sum_{i=1}^{n}\left|P_S^i - O_S^i\right|}{\sum_{i=1}^{n}\left|O_S^i - O_S\right|} \tag{17}$$

Wilmot's Index of Agreement (WI): WI, which ranges from 0 to 1, is a standardised index to measure the prediction efficacy of established models. A WI of 0 shows no match at all, whereas a WI of 1 shows complete agreement between predicted values and actual values. Equation (18) displays the WI definition.

$$WI = 1 - \frac{\sum_{i=1}^{n}\left|P_S^i - O_S^i\right|}{\sum_{i=1}^{n}\left|O_S^i - O_S\right|} \tag{18}$$

Where, O_S^i, P_S^i and n stands for i^{th} the observed value of settlement, i^{th} the anticipated value of settlement, and the quantity of data samples, respectively.

TABLE 2: Analysis of suggested models and other approaches based on statistical indices for comparison

Statistical index	ANN	HHO	CFA	MOA	Proposed
RMSE	0.813	0.586	0.512	0.481	0.352

MAE	0.44	0.321	0.28	0.26	0.22
Efficiency	0.963	0.974	0.977	0.98	0.985
RWI	0.897	0.885	0.905	0.933	0.951

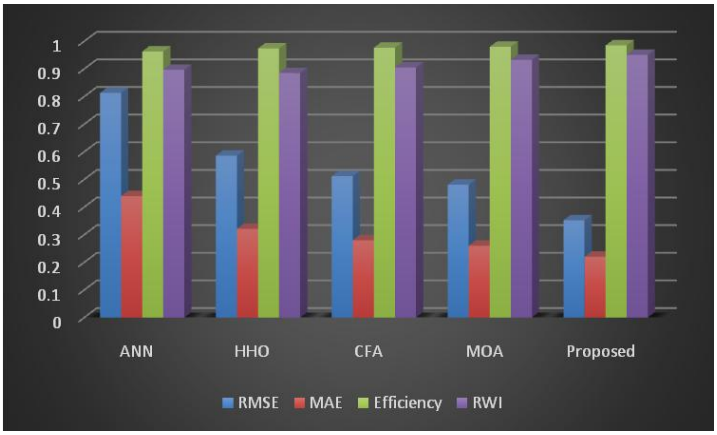

FIGURE 4: Performance analysis of statistical measurement

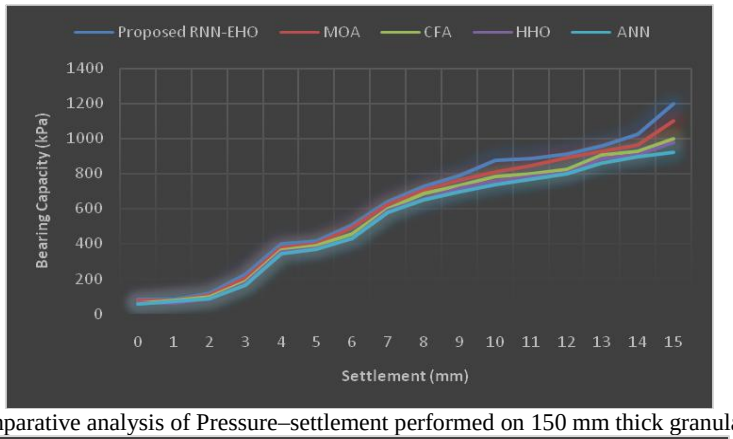

FIGURE 5: Comparative analysis of Pressure–settlement performed on 150 mm thick granular subbase layer

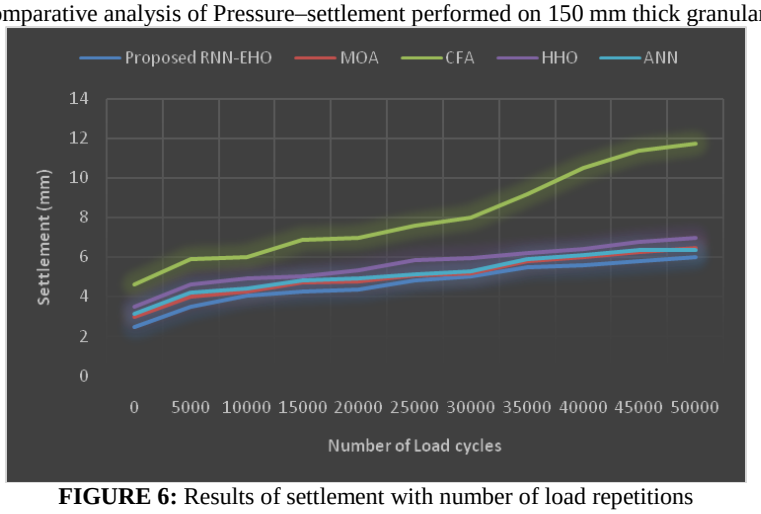

FIGURE 6: Results of settlement with number of load repetitions

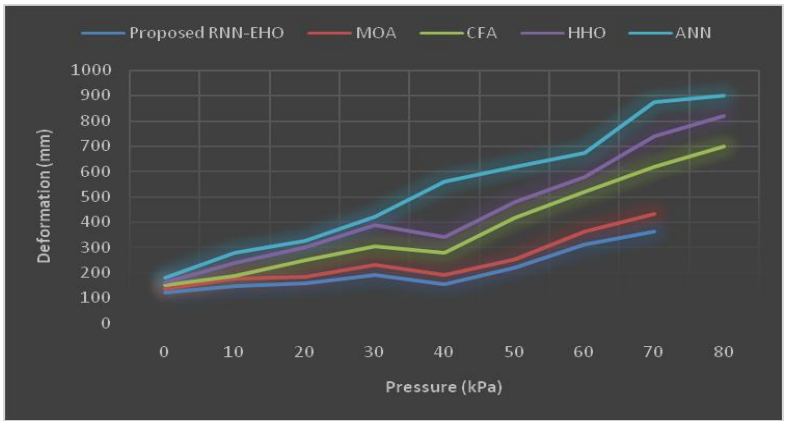

FIGURE 7: Showing comparison of deformation of exiting methods and proposed method at the centre with 120 mm thick base

Three different scenarios' pressure-settlement behaviors are compared in Fig. 5. The bearing capacity of the georgic reinforced foundation bed increased with the height of the georgic. Comparable observational methods that rely on numerical analysis. As the geocell's height increases, the footing load will be dispersed across a larger area. Figure 6 illustrates typical data on settlement variation for a 53 mm thick granular sub base layer with various geosynthetic reinforcement layer types. The results demonstrated that the initial modulus of the poor sand is relatively high; as settlement increased with the number of cycles, the modulus value decreased; and ultimately, near the conclusion of 22000 cycles, the modulus value stabilized at a constant value. Figure 7 shows that with geogrid of an 80 mm height, the ultimate bearing capacity of lime stone aggregate bases reinforced with geogrid increases by 1.1 times over unreinforced bases. Additionally, a 76 percent increase in the total bearing capacity augmentation factor was made. The findings show a significant increase in the performance of the suggested RNN-EHO approach employing Geogrid compared to other techniques such as ANN, CFA, MOA, and HHO, respectively, when the proposed method course was correctly compacted.

4. CONCLUSION

Analyses and pertinent results were attained by applying the georgic to the particular shape of a ballasted railway track substructure utilizing a verified recommended hybrid RNN-EHO technique. An analysis of its performance on real railways using realistic geometry and applications might be performed. Variations in ballast strength, foundation stiffness, and gorged stiffness were used in the analyses to mimic poorer track material, compressible sub grades, and the effects of reinforcing material on overall performance. To study the gorged-reinforced sand's improvement under static stress, a hybrid recurrent neural network (RNN)-elephant herding optimization (EHO) method was presented in this paper. The containment of the ballast using gorged was particularly efficient in decreasing vertical deformations, even when low-quality material was utilised, according to numerical modelling of geogrid applied to a train scenario. Lessening the requirement for reinforcement and substructure improvement results in greater ballast shear strength. Although the reduction in vertical settlement was not as large as anticipated, geogrid confinement was used. This is promising since it may allow for longer maintenance cycles when the ballast loses shear strength or the use of weaker ballast materials, including recycled ballast or well-graded particles. The reason for this is presumably that the subgrade experiences sizable pressures whether the geogrid is there or not. However, the geogrid did assist in more evenly distributing the loads, possibly preventing the development of substantial shear stresses and failure, especially on softer sub grades. By reducing the lateral ballast squeeze caused by large loads, the geogrid prevents vertical settlement on stronger foundations.

REFERENCES

[1]. Nguyen, Van Duc, et al. "Monitoring of an instrumented geosynthetic-reinforced piled embankment with a triangular pile configuration." International Journal of Rail Transportation (2022): 1-23.
[2]. Schary, Yitzchak. "Case studies on geocell-based reinforced roads, railways and ports." Geocells. Springer, Singapore, 2020. 387-411.
[3]. Deshpande, Tanmay D., et al. "Analysis of railway embankment supported with geosynthetic-encased stone columns in soft clays: a case study." International Journal of Geosynthetics and Ground Engineering 7.2 (2021): 1-16.
[4]. Lazorenko, Georgy, et al. "Failure analysis of widened railway embankment with different reinforcing measures under heavy axle loads: A comparative FEM study." Transportation Engineering 2 (2020): 100028.
[5]. Sweta, Kumari, and Syed KhajaKarimullahHussaini. "Effect of geogrid on deformation response and resilient modulus of railroad ballast under cyclic loading." Construction and Building Materials 264 (2020): 120690.
[6]. Hubballi, RajashekarMallikarjun. "Stabilization of Railway Tracks Using Geosynthetics—A Review." Proceedings of the 7th Indian Young Geotechnical Engineers Conference. Springer, Singapore, 2022.

[7]. Banerjee, Lalima, Sowmiya Chawla, and Sujit Kumar Dash. "Application of geocell reinforced coal mine overburden waste as subballast in railway tracks on weak subgrade." Construction and Building Materials 265 (2020): 120774.
[8]. Meena, Naveen Kumar, et al. "Effects of soil arching on behavior of pile-supported railway embankment: 2D FEM approach." Computers and Geotechnics 123 (2020): 103601.
[9]. Jain, Sanjaya Kumar, Mohammed Saleh Nusari, and Indra Prasad Acharya. "Use of geo-grid reinforcement and stone column for strengthening of mat foundation base." Materials Today: Proceedings (2020).
[10]. Mei, Yuan, et al. "Experimental study of the comprehensive technology of grouting and suspension under an operating railway in the cobble stratum." Transportation Geotechnics 30 (2021): 100612.
[11]. Ziegler, Martin. "Application of geogrid reinforced constructions: history, recent and future developments." Procedia Engineering 172 (2017): 42-51.
[12]. Yu, Zelong, et al. "True triaxial testing of geogrid for high speed railways." Transportation Geotechnics 20 (2019): 100247.
[13]. Esmaeili, Morteza, et al. "Investigating the effect of geogrid on stabilization of high railway embankments." Soils and Foundations 58.2 (2018): 319-332.
[14]. Zhang, Chonglei, Lijun Su, and Guanlu Jiang. "Full-scale model tests of load transfer in geogrid-reinforced and floating pile-supported embankments." Geotextiles and Geomembranes (2022).
[15]. Punetha, Piyush, and Sanjay Nimbalkar. "Performance improvement of ballasted railway tracks for high-speed rail operations." International Conference of the International Association for Computer Methods and Advances in Geomechanics. Springer, Cham, 2021.
[16]. Esen, A. F., et al. "Stress distribution in reinforced railway structures." Transportation Geotechnics 32 (2022): 100699.
[17]. Watanabe, Kenji, et al. "Construction and field measurement of high-speed railway test embankment built on Indian expansive soil “Black Cotton Soil”." Soils and Foundations 61.1 (2021): 218-238.
[18]. Bonatti, Colin, and Dirk Mohr. "On the importance of self-consistency in recurrent neural network models representing elasto-plastic solids." Journal of the Mechanics and Physics of Solids 158 (2022): 104697.
[19]. Li, Wei, and Gai-Ge Wang. "Elephant herding optimization using dynamic topology and biogeography-based optimization based on learning for numerical optimization." Engineering with Computers 38.2 (2022): 1585-1613.
[20]. Guptha, Nirmala S., et al. "Cross lingual handwritten character recognition using long short term memory network with aid of elephant herding optimization algorithm." Pattern Recognition Letters 159 (2022): 16-22.

